
Learning from Suboptimal Data in Continuous Control via Auto-Regressive Soft Q-Network

Jijia Liu¹ Feng Gao¹ Qingmin Liao¹ Chao Yu¹ Yu Wang¹

Abstract

Reinforcement learning (RL) for continuous control often requires large amounts of online interaction data. Value-based RL methods can mitigate this burden by offering relatively high sample efficiency. Some studies further enhance sample efficiency by incorporating offline demonstration data to “kick-start” training, achieving promising results in continuous control. However, they typically compute the Q-function independently for each action dimension, neglecting interdependencies and making it harder to identify optimal actions when learning from suboptimal data, such as non-expert demonstration and online-collected data during the training process. To address these issues, we propose *Auto-Regressive Soft Q-learning* (ARSQ), a value-based RL algorithm that models Q-values in a coarse-to-fine, auto-regressive manner. First, ARSQ decomposes the continuous action space into discrete spaces in a coarse-to-fine hierarchy, enhancing sample efficiency for fine-grained continuous control tasks. Next, it auto-regressively predicts dimensional action advantages within each decision step, enabling more effective decision-making in continuous control tasks. We evaluate ARSQ on two continuous control benchmarks, RL Bench and D4RL, integrating demonstration data into online training. On D4RL, which includes non-expert demonstrations, ARSQ achieves an average $1.62\times$ performance improvement over SOTA value-based baseline. On RL Bench, which incorporates expert demonstrations, ARSQ surpasses various baselines, demonstrating its effectiveness in learning from suboptimal online-collected data.

1. Introduction

Deep reinforcement learning (RL) has demonstrated remarkable performance across various continuous control domains (Haarnoja et al., 2018; Schulman et al., 2017). However, these breakthroughs often come at the cost of extensive online interactions, which are required for effective convergence (Berner et al., 2019; Mnih et al., 2015). This reliance on large-scale exploration poses a major challenge in real-world applications, where data collection can be expensive, time-consuming, or even risky. To alleviate this burden, value-based RL methods, which directly approximate the Q-function rather than parameterizing a policy, have gained popularity due to their improved sample efficiency (Seyde et al., 2024; Tavakoli et al., 2020; Seyde et al., 2022) and have shown advances in continuous control tasks by discretizing each of the dimensions of continuous action spaces. (Seo et al., 2024). Moreover, some studies integrate offline demonstration data into training to further accelerate early learning, reducing the dependence on purely online exploration (Ball et al., 2023). In this paper, we adopt this training paradigm to address continuous control using value-based RL, incorporating offline data into the online training process.

For value-based RL, the discretization scheme results in an exponentially large discrete action space, making RL training and exploration challenging. To mitigate this, existing value-based methods often estimate the Q-value for each action dimension independently (Metz et al., 2017; Seyde et al., 2022). However, this simplification comes with a limitation—it neglects interdependencies between action dimensions, potentially leading to suboptimal decision-making. When training data exhibits multiple modes, such as a mix of optimal and suboptimal demonstrations, independently estimating Q-values can bias action selection toward the most frequent behaviors rather than the truly optimal ones. This limitation is particularly pronounced in the early stages of learning, when the agent relies heavily on imperfect offline data and lacks sufficient online refinement.

Consider a simple one-step decision-making task with two-dimensional actions $(a_1, a_2) \in \mathcal{A} = [-1, 1]^2 \subset \mathbb{R}^2$, shown in Fig. 1, where an agent selects an action (a_1, a_2) given state s and receives a reward r before the episode terminates.

¹Tsinghua University, Beijing, China. Correspondence to: Chao Yu <zoeyuchao@gmail.com>, Yu Wang <yu-wang@tsinghua.edu.cn>.

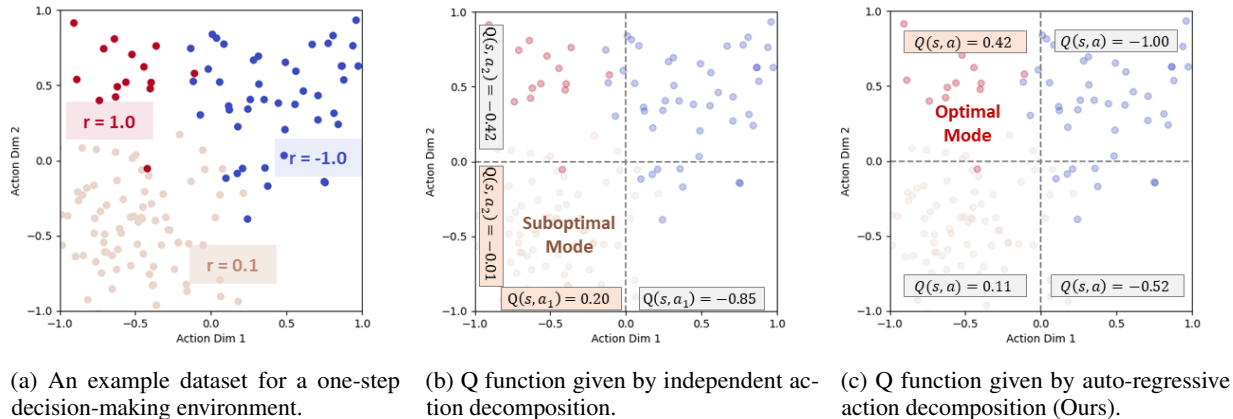


Figure 1. A motivating example of how Q decomposition influences policy training, as detailed in Appendix C.1.

Suppose the training dataset consists of three distinct modes: one optimal mode with $r = 1$, two suboptimal modes with $r = 0.1$ and $r = -1$, with the latter occurring more frequently. If the suboptimal modes are more prevalent in the dataset, conventional Q-learning approaches that estimate action dimensions independently, i.e., $Q(s, a_i)$, could undervalue the optimal mode. This bias can hinder the correct identification and reinforcement of the optimal action mode, leading to slow convergence and degraded policy performance.

To address this issue, we propose *Auto-Regressive Soft Q-learning* (ARSQ), a novel approach that captures cross-dimensional dependencies in discretized high-dimensional action spaces. Instead of treating each dimension independently, ARSQ adopts an auto-regressive structure, sequentially estimating advantages for each action dimension conditioned on the previously selected dimensions. This allows the method to better model interdependencies, ensuring that correlated action dimensions are jointly optimized rather than selected in isolation. Additionally, ARSQ adopts a coarse-to-fine hierarchical discretization strategy inspired by CQN (Seo et al., 2024), further enhancing sample efficiency for fine-grained continuous control. We theoretically show that the original Q function can be expanded into an auto-regressive formulation with dimensional advantage estimation under the framework of soft Q-learning. Our approach integrates these insights into an auto-regressive soft Q-network, which is specifically designed for continuous control tasks.

To evaluate ARSQ, we conduct extensive experiments on the D4RL and RLbench continuous control benchmarks, challenging it against a variety of widely used reinforcement learning and imitation learning baselines. Results indicate that ARSQ consistently surpasses these baselines, achieving up to $1.62\times$ performance over existing value-based RL

when trained with suboptimal demonstrations on D4RL. Ablation studies further highlight the significance of ARSQ’s key components, confirming its effectiveness in continuous control tasks.

Our contributions include:

- We extend Soft Q-learning framework to value-based reinforcement learning with dimensional advantage estimation.
- We propose the ARSQ algorithm to capture dependencies in action dimensions and enhance learning from suboptimal data.
- Through extensive experiments, we demonstrate that ARSQ can learn better policies when data suboptimality arises from either offline datasets or data collected online.

2. Related Works

Value-based RL for Continuous Control. Despite their inherently straightforward critic-only framework, value-based reinforcement learning (RL) algorithms have achieved notable success (Mnih et al., 2015; Silver et al., 2017; Schrittwieser et al., 2020; Seyde et al., 2024; Seo et al., 2024). Although these algorithms are primarily designed for discrete action spaces, recent efforts have sought to adapt them to continuous control by discretizing the continuous action space (Tavakoli et al., 2018; Seyde et al., 2022). However, the curse of dimensionality remains a significant challenge, as the number of discretization bins increases exponentially with the action dimension (Lillicrap, 2015). To address this issue, some studies have modified the Markov Decision Process (MDP) of the environment, transforming it into a sequential decision-making problem along the action dimension (Metz et al., 2017; Chebotar et al., 2023). Other ap-

proaches treat each action dimension independently, generating the Q function separately for each dimension (Tavakoli et al., 2018; 2020; Seyde et al., 2022; 2024), akin to treating each action dimension as a multi-agent RL problem (Foerster et al., 2018; Yu et al., 2022). Recent research (Seo et al., 2024) has employed a coarse-to-fine discretization approach to improve sample efficiency. However, treating each action dimension independently may disrupt the correlation between different action dimensions, potentially diminishing performance in policy optimization. Some studies (Seo & Abbeel, 2024) have attempted to solve this issue through action sequence prediction. Our approach generates actions in an auto-regressive manner, considering the correlations between dimensions and improving policy learning, which is orthogonal to (Seo & Abbeel, 2024).

Online RL with Offline Demonstration. Deep reinforcement learning often requires a large amount of online interactions to achieve convergence (Berner et al., 2019; Mnih et al., 2015). To address this challenge, many methods have been proposed that leverage offline demonstrations to guide online exploration and accelerate policy training (Rajeswaran et al., 2017; Ball et al., 2023). Some approaches involve performing offline RL pretraining before initiating online RL training (Lee et al., 2022; Nakamoto et al., 2024; Lei et al., 2023; Hu et al., 2024). However, these approaches often depend on expensive offline pretraining. To mitigate this, some works explore incorporating offline demonstration data directly into the training process. One strategy initializes the replay buffer with offline data (Hester et al., 2018; Ball et al., 2023), while another balances sampling between online and offline data to improve training stability (Zhang et al., 2023; Hansen et al., 2022). Additionally, certain methods explicitly introduce a behavior cloning loss to leverage high-quality demonstrations for better guidance (Rudner et al., 2021; Rajeswaran et al., 2017; Nair et al., 2018). In this work, we adopt the paradigm of integrating offline demonstrations into training to enhance sample efficiency in continuous control tasks. Specifically, we improve value-based RL by introducing an auto-regressive structure that sequentially estimates advantage for each action dimension. This design enables better handling of suboptimal data, whether from offline demonstrations or trajectories collected during training.

3. Preliminaries

3.1. Problem Formulation

In this paper, we consider the standard RL setting with the addition of a pre-collected dataset \mathcal{D} for continuous control. The problem can be represented as MDP, defined by the tuple $(\mathcal{S}, \mathcal{A}, \gamma, p, r, d_0)$. Here, \mathcal{S} is the continuous state space, \mathcal{A} is the continuous action space, $\gamma \in (0, 1)$ is the discount factor, $p(s' | s, a)$ is the transition dynamics,

$r(s, a)$ is the reward function, and $d_0(s)$ is the distribution of the initial state. In addition to interacting with the environment online, we assume access to a pre-collected dataset $\mathcal{D} = \{(s_i, a_i, r_i, s'_i)\}$, which can substantially reduce sample complexity and provide broader state-action coverage.

3.2. Soft Q Learning

To improve policy exploration, maximum entropy RL enhances the reward by adding an entropy term (Ziebart et al., 2008; Haarnoja et al., 2017; 2018), so the optimal policy seeks to maximize entropy at every state it visits. The objective is defined as

$$J(\pi) = \sum_{t=0}^T \mathbb{E}_{(s_t, \mathbf{a}_t) \sim \rho_\pi} [r(s_t, \mathbf{a}_t) + \alpha \mathcal{H}(\pi(\cdot | s_t))] \quad (1)$$

where \mathcal{H} is entropy, T is the episode length and ρ_π is the trajectory distribution induced by policy π . The temperature parameter α dictates how much importance is placed on the entropy term in comparison to the reward. Let the soft Q-function defined as:

$$Q_{\text{soft}}^*(s_t, \mathbf{a}_t) = r_t + \mathbb{E}_{(s_{t+1}, \dots) \sim \rho_\pi} \left[\sum_{l=1}^{\infty} \gamma^l (r_{t+l} + \alpha H(\pi^*(\cdot | s_{t+l}))) \right] \quad (2)$$

Then the optimal policy for Eq. (1) is given by

$$\pi^*(\mathbf{a}_t | s_t) = \exp \left(\frac{1}{\alpha} (Q_{\text{soft}}^*(s_t, \mathbf{a}_t) - V_{\text{soft}}^*(s_t)) \right) \quad (3)$$

$$V_{\text{soft}}^*(s_t) = \alpha \log \int_{\mathcal{A}} \exp \left(\frac{1}{\alpha} Q_{\text{soft}}^*(s_t, \mathbf{a}') \right) d\mathbf{a}' \quad (4)$$

Similar to the standard Q-function and value function, the Q-function can be connected to the value function at a future state using a soft Bellman equation.

$$Q_{\text{soft}}^*(s_t, \mathbf{a}_t) = r_t + \gamma \mathbb{E}_{s_{t+1} \sim p(s_{t+1}, \mathbf{a}_t)} [V_{\text{soft}}^*(s_{t+1})] \quad (5)$$

The proof can be found in (Ziebart et al., 2008; Haarnoja et al., 2017).

4. Method

In this section, we begin by discussing the process of discretizing multi-dimensional actions in a coarse-to-fine manner. Building on this, we extend the soft Q-learning theory with a focus on the dimensional soft advantage. Subsequently, we introduce our *Auto-Regressive Soft Q-learning* (ARSQ) algorithm, which is overviewed in Fig. 2.

4.1. Coarse-to-fine Action Discretization

To apply Q-learning (Mnih et al., 2015) in a continuous domain, a straightforward approach is to discretize the action space (Tang & Agrawal, 2020; Seo et al., 2024). For a

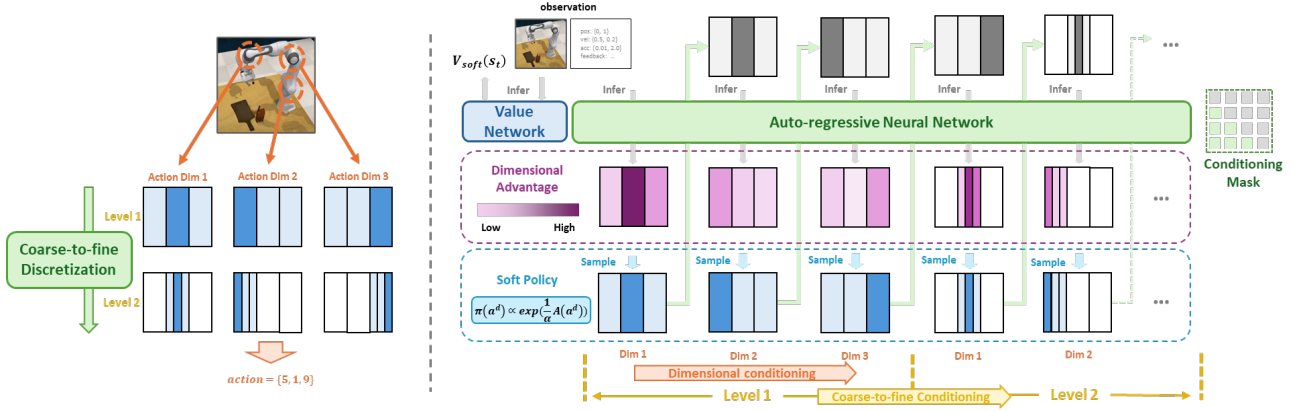


Figure 2. The ARSQ algorithm. The action space is discretized using a coarse-to-fine approach. By predicting dimensional soft advantages, ARSQ generates actions in an auto-regressive manner within a single decision-making step.

continuous action of d dimensions $\mathbf{a}_c = (a_c^1, a_c^2, \dots, a_c^d) \in \mathbb{R}^D$, the discretized action $\mathbf{a} = (a^1, a^2, \dots, a^d)$ can be represented by

$$a^d = \arg \max_i |a_c^d - b_i| \quad (6)$$

where $\mathbf{b} = (b_1, \dots, b_B)$ are the centers of B discretization intervals, or bins, which typically provide a uniform separation of the given action space. However, obtaining a finer separation of the action space necessitates a greater number of bins, thereby increasing the computational load when assessing the Q function for each discrete action bin.

To address this issue, we can apply a coarse-to-fine action discretization approach (Seo et al., 2024), similar to the method used in (Yan et al., 2015) for computer vision, as illustrated in Fig. 2. With L levels and B uniform separation bins at each level, the discrete action for dimension d at level l is expressed as:

$$a^{d,l} = \lfloor \frac{a^d - \sum_{i=1}^{l-1} B^{L-i} a^{d,i}}{B^{L-l}} \rfloor \quad (7)$$

Here, $\lfloor \cdot \rfloor$ represents the floor function.

During inference, the policy generates discrete actions progressively through each level ($\mathbf{a}^{(\cdot),1}, \mathbf{a}^{(\cdot),2}, \dots, \mathbf{a}^{(\cdot),L}$). These are then combined to produce the final discrete action.

4.2. Dimensional Soft Advantage for Policy Representation

Building on action discretization, we initially extend soft Q-learning to discrete spaces. The soft value function is expressed as

$$V_{\text{soft}}^*(\mathbf{s}) = \alpha \log \sum_{\mathbf{a}' \in \mathcal{A}} \exp\left(\frac{1}{\alpha} Q_{\text{soft}}^*(\mathbf{s}, \mathbf{a}')\right) \quad (8)$$

And we omit the subscript t for \mathbf{s}_t and \mathbf{a}_t . To further streamline the expression of the policy, we define the soft advantage.

Definition 4.1 (Soft Advantage). The soft advantage of \mathbf{a} at \mathbf{s} is given by

$$A^*(\mathbf{s}, \mathbf{a}) = Q_{\text{soft}}^*(\mathbf{s}, \mathbf{a}) - V_{\text{soft}}^*(\mathbf{s}) \quad (9)$$

Similar to the advantage in policy gradient-based RL algorithms, the soft advantage assesses how much taking action \mathbf{a} at state \mathbf{s} is beneficial. Thus, the optimal policy in Eq. (3) can be expressed as

$$\pi^*(\mathbf{a}|\mathbf{s}) = \exp\left(\frac{1}{\alpha} A^*(\mathbf{s}, \mathbf{a})\right) \quad (10)$$

Considering the multi-dimensional action space, it still remains necessary to use a neural network to output $B^{L \times D}$ Q values in the final layer, as per the DQN (Mnih et al., 2015).

However, outputting such a large number of Q values imposes a significant computational burden on the neural network. Inspired by auto-regression (Brown et al., 2020), we address this problem by generating the Q function for a state-action pair in an auto-regressive manner.

For clarity, we treat discrete action discussed in Sec. 4.1 in one level. The multi-level coarse-to-fine discrete action can be considered as additional action dimensions, without compromising generalization. We first define the dimensional soft advantage for policy representation.

Definition 4.2 (Dimensional Soft Advantage). The dimensional soft advantage of the action a^d at state \mathbf{s} , considering the previous dimensional actions $\mathbf{a}^{-d} = (a^1, \dots, a^{d-1})$, is expressed by

$$\pi(a^d|\mathbf{s}, \mathbf{a}^{-d}) = \frac{\exp\left(\frac{1}{\alpha} A^d(\mathbf{s}, \mathbf{a}^{-d}, a^d)\right)}{Z(\mathbf{s}, \mathbf{a}^{-d})} \quad (11)$$

where $Z^d(\mathbf{s}, \mathbf{a}^{-d})$ represents the partition function.

However, the dimensional soft advantage is not related to other equations and remains intractable. To address this, we propose the following theorem to establish a connection between the dimensional soft advantage and the soft advantage.

Theorem 4.3. *If dimensional soft advantage $m^d(\mathbf{s}, \mathbf{a}^{-d}, a^d)$ satisfies*

$$\log \sum_{a^{d'}} \exp\left(\frac{1}{\alpha} A^d(\mathbf{s}, \mathbf{a}^{-d}, a^{d'})\right) = 0 \quad (12)$$

then the soft advantage can then be expressed as the summation of the dimensional soft advantages

$$\sum_{d=1}^D A^d(\mathbf{s}, \mathbf{a}^{-d}, a^d) = A(\mathbf{s}, \mathbf{a}) \quad (13)$$

Proof. See Appendix A. \square

Through Eq. (11) and Theorem 4.3, we extend soft Q-learning to a auto-regressive policy along action dimension.

Since we do not introduce additional elements in policy optimization, the Q-iteration follows the same update rule as soft Q-learning. Based on Eq. (5), we have

$$V_{\text{soft}}(\mathbf{s}_t) + A(\mathbf{s}_t, \mathbf{a}_t) \leftarrow r_t + \gamma \mathbb{E}_{\mathbf{s}_{t+1} \sim p(\mathbf{s})} [V_{\text{soft}}(\mathbf{s}_{t+1})] \quad (14)$$

The maximum entropy policy described in Eq. (3) can be obtained by repeatedly applying Eq. (14) until it converges.

4.3. Auto-Regressive Soft Q-learning

Building on the theory outlined in Sec. 4.2, we introduce the *Auto-Regressive Soft Q-learning* (ARSQ) algorithm. The pseudo code for the ARSQ algorithm is presented in Algorithm 1. We will discuss the various design choices of ARSQ.

Behavior cloning objective. To leverage offline demonstration data during online training, we introduce an additional behavior cloning loss term. Following previous works (Hester et al., 2018; Seo et al., 2024), we encourage actions present in the offline dataset to be preferred over other actions. Specifically, we define the loss as

$$\mathcal{L}_{BC}^d = \sum_{a^d} \max(A^{d,\theta_i}(\mathbf{s}, \mathbf{a}_e^{-d}, a^d) - A^{d,\theta_i}(\mathbf{s}, \mathbf{a}_e^{-d}, a_e^d), C_m) \quad (15)$$

where \mathbf{a}_e denotes the expert action observed in the offline dataset, and C_m is a hyper-parameter controlling the margin. This objective encourages the soft advantages of expert actions to be at least C_m higher than those of other actions.

Algorithm 1 Auto-Regressive Soft Q Algorithm (ARSQ)

```

Initialize  $\theta_{1,2}, \phi_{1,2}$  for  $A^{\theta_i}$  and  $V_{\text{soft}}^{\phi_i}$ 
Assign target parameters  $\bar{\theta}_i, \bar{\phi}_i \leftarrow \theta_i, \phi_i$ .
Offline dataset  $\mathcal{D}$ , replay buffer  $\mathcal{R} \leftarrow \mathcal{D}$ .
for each epoch do
  for each environment step do
    select  $\mathbf{a}_t$  with  $A_{\theta_1}$  and  $A_{\theta_2}$  (10, 16)
     $\mathbf{s}_{t+1} \sim p(\mathbf{s}_{t+1} | \mathbf{s}_t, \mathbf{a}_t)$ 
     $\mathcal{R} \leftarrow \mathcal{R} \cup \{\mathbf{s}_t, \mathbf{a}_t, r_t, \mathbf{s}_{t+1}\}$ 
  end for
  for each gradient step do
    Sample mini-batch  $b_D, b_R$  from  $\mathcal{D}, \mathcal{R}$ 
    Calculate  $\mathcal{L}_D = \mathcal{L}_{RL} + \beta \mathcal{L}_{BC}$  with  $b_D$  (15, 18)
    Calculate  $\mathcal{L}_R = \mathcal{L}_{RL}$  with  $b_R$  (18)
    Update  $m_{\theta_i}$  according to  $\hat{\nabla}_{\theta_i}(\mathcal{L}_D + \mathcal{L}_R)$ 
    Update  $V_{s,\phi_i}$  according to  $\hat{\nabla}_{\phi_i}(\mathcal{L}_D + \mathcal{L}_R)$ 
    Update target networks  $\bar{\theta}_i \leftarrow \rho \bar{\theta}_i + (1 - \rho)\theta_i$  and
     $\bar{\phi}_i \leftarrow \rho \bar{\phi}_i + (1 - \rho)\phi_i$ .
  end for
end for
    
```

Policy representation. As discussed in Sec. 4.2, ARSQ predicts dimensional soft advantages, which function as both components of the Q function and policy representation. The network architecture is illustrated in Fig. 3. In practical design, the soft value V_{soft} and the dimensional soft advantage A^d are predicted using two separate neural networks. The advantage prediction network estimates the dimensional soft advantage for each action dimension, based on the partially generated action from previous dimensions, creating an auto-regressive sequence. In practical design, we use a globally-shared MLP in the advantage network, with separate heads to predict the dimensional soft advantages.

Another challenge is applying the constraint of the dimensional soft advantage as per Eq. (12). Here, we enforce a hard constraint by normalizing each output head through log-sum-exp subtraction, ensuring consistency across outputs.

$$A^d(\mathbf{s}_t, \mathbf{a}^{-d}, a^d) = u^d(\mathbf{s}_t, \mathbf{a}^{-d}, a^d) - \log \sum_{a^{d'}} \exp\left(\frac{1}{\alpha} u^d(\mathbf{s}_t, \mathbf{a}^{-d}, a^{d'})\right) \quad (16)$$

where u^d is the output of the d -th output head.

Furthermore, to stabilize training and address the over-estimation problem (Fujimoto et al., 2018; Van Hasselt et al., 2016), we implemented a double Q network alongside a target network in our practical application. Therefore, the

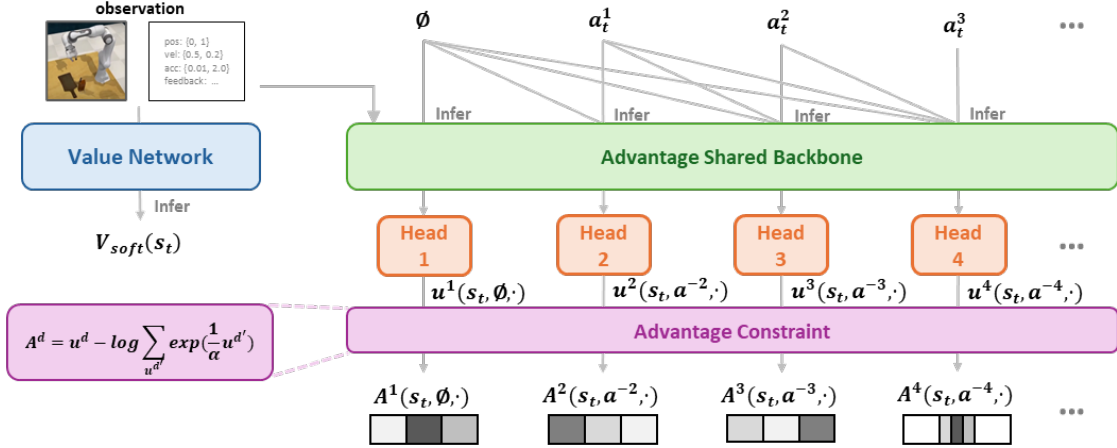


Figure 3. Network architecture of ARSQ. The soft value V_{soft} and the dimensional soft advantage A^d are predicted by two separate networks. The advantage network utilizes a shared backbone, and advantage constraints are applied to its output.

optimization objective in Eq. (14) is modified to

$$\mathbf{y}_t = \gamma \mathbb{E}_{\mathbf{s}_{t+1} \sim p(\mathbf{s})} \left[\min \left(V_{\text{soft}1}^{\bar{\phi}_1}(\mathbf{s}_{t+1}), V_{\text{soft}2}^{\bar{\phi}_2}(\mathbf{s}_{t+1}) \right) \right] \quad (17)$$

$$\mathcal{L}_{RL} = \frac{1}{2} \left(V_{\text{soft}}^{\phi_i}(\mathbf{s}_t) + A^{\theta_i}(\mathbf{s}_t, \mathbf{a}_t) - \mathbf{y}_t \right) \quad (18)$$

where $V_{\text{soft}}^{\bar{\phi}_i}$ represents the soft value predicted by the target network.

Auto-regressive conditioning. In Sec. 4.2, we explained the process of handling discrete action in one coarse-to-fine level. With multi-level coarse-to-fine action discretization, the auto-regressive conditioning encompasses two aspects. *Dimensional conditioning* refers to generating actions for each dimension in an auto-regressive sequence, while *coarse-to-fine conditioning* involves generating actions for each dimension from coarse to fine. In practice, we implement coarse-to-fine conditioning prior to dimensional conditioning. Specifically, dimensional conditioning serves as the inner conditioning, while coarse-to-fine conditioning acts as the outer conditioning across levels. We explore swapping the order of conditioning in Sec. 5.3, and the results indicate that the current design better captures interdependencies between action dimensions.

5. Experiment

We design our experiments to investigate the following questions: (i) What is ARSQ’s performance when the offline dataset is suboptimal? (ii) What is ARSQ’s performance when online collected data is suboptimal? (iii) How do various design factors of ARSQ affect the performance?

Benchmarks. We evaluate our approach on two continuous control benchmarks: D4RL (Fu et al., 2020) and RL Bench (James et al., 2020). Both domains provide access to online

interaction data and a limited number of demonstrations, enabling us to assess the performance of ARSQ in diverse settings. We present representative results here due to limited space and leave full results in Appendix D.

Baselines. We use CQN (Seo et al., 2024), a state-of-the-art value-based RL method for continuous control, as our baseline. CQN employs a coarse-to-fine action selection strategy and independently predicts Q-values for each action dimension. Additionally, CQN trains using a combination of online training and offline demonstrations. Besides, we also include DrQ-v2 (Yarats et al., 2021), a renowned actor-critic algorithm designed for vision-based RL, along with its enhanced version, DrQ-v2+, as benchmarks. We also feature ACT (Zhao et al., 2023) and a CQN-style behavior cloning (BC) policy among our baselines. Details about the baselines can be found in Appendix C.3.

5.1. Performance on D4RL

Main results. To evaluate ARSQ’s performance when the offline dataset is suboptimal, we consider three distinct locomotion tasks from the D4RL benchmark, each with three datasets of varying quality. The *medium* dataset is gathered using a medium-level policy, whereas the *medium-expert* dataset comprises a combination of medium-level and expert demonstrations. The *medium-replay* dataset includes data ranging from completely random to medium-level. The input to the model consists of state representations, while the output corresponds to torques applied at each hinge joint. A dense reward is provided to encourage completing the task, staying alive, and discourage vigorous actions that consume excessive energy.

We evaluate ARSQ, CQN (Seo et al., 2024), and BC in this setting. At the beginning of online training, the replay buffer for both ARSQ and CQN is initialized with an offline

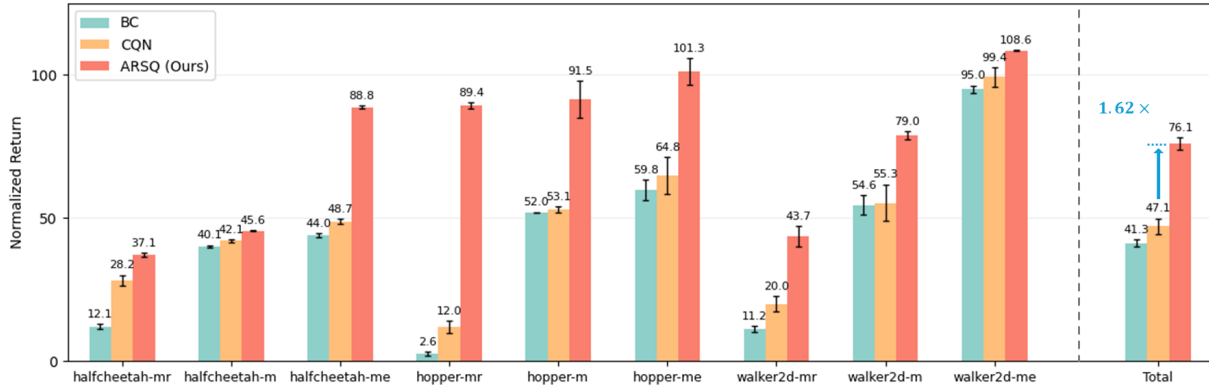


Figure 4. D4RL main results. *mr*, *m*, and *me* represent *medium-replay*, *medium*, and *medium-expert*, respectively.

dataset, and online data is added as the training progresses. Additionally, both ARSQ and CQN incorporate the BC objective (Eq. (15)) towards offline dataset. The BC baseline is trained solely offline using the offline dataset with the BC objective. We report the converged performance of ARSQ, CQN and BC, averaged over three random seeds.

As shown in Fig. 4, ARSQ exhibits outstanding performance across all nine datasets, demonstrating its ability to effectively identify suboptimal actions and learn more efficiently from the available offline data. ARSQ surpasses CQN, particularly in the *medium-replay* and *medium-expert* datasets, where optimal data is not predominant, highlighting that ARSQ is less biased toward frequently observed suboptimal actions. Notably, both ARSQ and CQN outperform BC, indicating that conducting reinforcement learning online enhances policy performance.

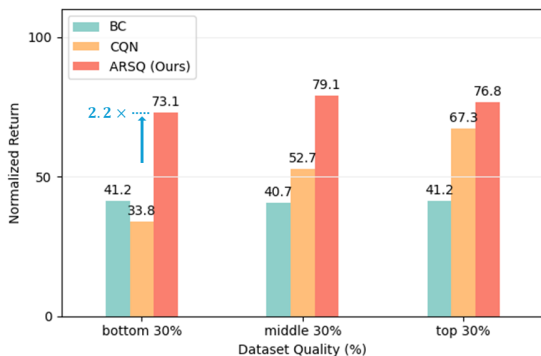


Figure 5. D4RL results on different demonstration quality averaged over 3 tasks, with each task containing 3 datasets respectively. We report the normalized return provided by D4RL.

Analysis on demonstration quality. To better investigate the influence of dataset quality, we rank trajectories by episode return for each dataset, and labeling the top 30%, middle 30%, and bottom 30% of the data as offline demonstrations. The behavior cloning objective is applied only to these offline demonstrations. We report the converged

performance ARSQ, CQN and BC. As illustrated in Fig. 5, ARSQ consistently outperforms both CQN and BC across all three levels of demonstration quality. Notably, when using the bottom 30% of data as offline demonstrations, ARSQ achieves approximately $2.2\times$ the final performance of CQN. In contrast, with the lowest demonstration quality, CQN performs slightly worse than BC, revealing CQN’s sensitivity to demonstration quality, which negatively affects its online training. These results further validate the effectiveness of our method when using suboptimal offline datasets.

5.2. Performance on RL Bench

To further evaluate ARSQ’s performance, we focus on six tasks from RL Bench (James et al., 2020). The agent receives input as RGB images and proprioceptive states and outputs the change in joint angles to control the robot arm. Unlike D4RL, the reward is sparse, offering a binary value (0 or 1) only at the final timestamp. Although each task is provided with 100 expert demonstrations, the agent might gather unsuccessful trajectories during its interaction with the environment. This setup allows us to examine the performance when the data collected online is suboptimal.

In this domain, we evaluate the performance of ARSQ, CQN, DrQ-v2+, DrQ-v2, ACT and BC. All reinforcement learning methods incorporate the behavior cloning objective (Eq. (15)) towards expert demonstrations and successful trajectories collected online.

As shown in Fig. 6, ARSQ demonstrates superior performance compared to all other algorithms, highlighting its effectiveness in online learning with suboptimal collected data. Additionally, ARSQ exceeds ACT, highlighting the importance of reinforcement learning in online training.

5.3. Ablation Studies

In this section, we evaluate the impact of key design factors in ARSQ: auto-regressive conditioning (Fig.2) and advan-

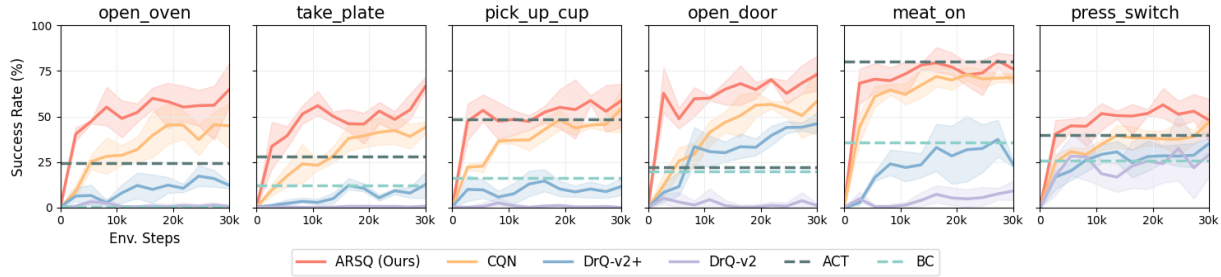


Figure 6. RL Bench results on different tasks. Each experiment begins with 100 expert demonstrations, and all RL methods include a behavior cloning objective.

tage prediction network (Fig.3).

Ablation on auto-regressive conditioning We consider several variants of ARSQ on auto-regressive conditioning.

- *Swap*: We reverse the conditioning order, applying dimensional conditioning first, followed by coarse-to-fine conditioning.
- *w/o CF Cond.*: We remove the coarse-to-fine conditioning and output actions at multiple levels simultaneously.
- *w/o Dim Cond.*: We remove the dimensional conditioning and instead output all action dimensions simultaneously at each level.
- *w/o CF*: We replace the coarse-to-fine structure entirely by discretizing each action dimension into B^L bins and then applying dimensional conditioning.
- *Plain*: We remove both the coarse-to-fine structure and dimensional conditioning.

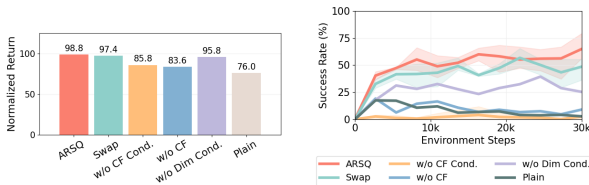


Figure 7. Ablation on auto-regressive conditioning in D4RL (left) and RL Bench (right).

As depicted in Fig. 7, *Swap* demonstrates a slight decline in performance, underscoring the effectiveness of the current conditioning order design. Additionally, removing any of the components degrades performance to varying degrees. When all components are removed, as in *Plain*, the performance is at its lowest, emphasizing the significance of dimensional and coarse-to-fine action generation.

Ablation on shared backbone. The advantage network of ARSQ utilizes a shared backbone to reduce the number of parameters and speed up the learning process. To assess the impact of this choice, we introduce two variants. The

network architecture of these two variants can be found in Appendix C.3.

- *Separate*: We employ separate networks for each action dimension.
- *Level Shared*: We employ shared networks for each coarse-to-fine level.

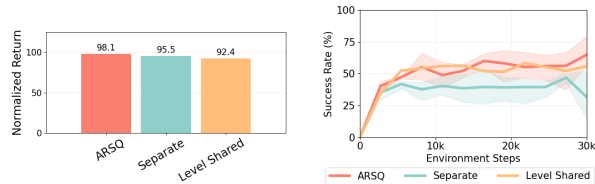


Figure 8. Ablation on shared backbone in D4RL (left) and RL-Bench (right).

As shown in Fig. 8, the standard ARSQ consistently performs well in both environments. In contrast, using either a level-shared or separate backbone results in diminished performance. This demonstrates the effectiveness of the shared backbone design.

6. Conclusion

In this paper, we introduced *Auto-Regressive Soft Q-learning* (ARSQ), a novel value-based RL approach tailored for continuous control tasks with suboptimal data. ARSQ addresses the limitations of existing value-based methods by adopting an auto-regressive structure that sequentially estimates soft advantage for each action dimension, thereby capturing cross-dimensional dependencies. Through empirical evaluations, we show that ARSQ significantly surpasses existing methods, highlighting its effectiveness in learning from suboptimal data.

For future directions, an adaptive coarse-to-fine discretization can be used to balance control granularity with the overhead of additional bins. Another approach to explore is grouping unrelated dimensions to shorten the conditioning chain length, thereby speeding up computation.

Impact Statement

This paper presents work whose goal is to advance the field of Machine Learning. There are many potential societal consequences of our work, none which we feel must be specifically highlighted here.

References

- Ba, J. L. Layer normalization. *arXiv preprint arXiv:1607.06450*, 2016.
- Ball, P. J., Smith, L., Kostrikov, I., and Levine, S. Efficient online reinforcement learning with offline data. In *International Conference on Machine Learning*, pp. 1577–1594. PMLR, 2023.
- Berner, C., Brockman, G., Chan, B., Cheung, V., Debiak, P., Dennison, C., Farhi, D., Fischer, Q., Hashme, S., Hesse, C., et al. Dota 2 with large scale deep reinforcement learning. *arXiv preprint arXiv:1912.06680*, 2019.
- Brown, T., Mann, B., Ryder, N., Subbiah, M., Kaplan, J. D., Dhariwal, P., Neelakantan, A., Shyam, P., Sastry, G., Askell, A., et al. Language models are few-shot learners. *Advances in neural information processing systems*, 33: 1877–1901, 2020.
- Chebotar, Y., Vuong, Q., Hausman, K., Xia, F., Lu, Y., Irpan, A., Kumar, A., Yu, T., Herzog, A., Pertsch, K., et al. Q-transformer: Scalable offline reinforcement learning via autoregressive q-functions. In *Conference on Robot Learning*, pp. 3909–3928. PMLR, 2023.
- Foerster, J., Farquhar, G., Afouras, T., Nardelli, N., and Whiteson, S. Counterfactual multi-agent policy gradients. In *Proceedings of the AAAI conference on artificial intelligence*, volume 32, 2018.
- Fu, J., Kumar, A., Nachum, O., Tucker, G., and Levine, S. D4rl: Datasets for deep data-driven reinforcement learning. *arXiv preprint arXiv:2004.07219*, 2020.
- Fujimoto, S., Hoof, H., and Meger, D. Addressing function approximation error in actor-critic methods. In *International conference on machine learning*, pp. 1587–1596. PMLR, 2018.
- Haarnoja, T., Tang, H., Abbeel, P., and Levine, S. Reinforcement learning with deep energy-based policies. In *International conference on machine learning*, pp. 1352–1361. PMLR, 2017.
- Haarnoja, T., Zhou, A., Abbeel, P., and Levine, S. Soft actor-critic: Off-policy maximum entropy deep reinforcement learning with a stochastic actor. In *International conference on machine learning*, pp. 1861–1870. PMLR, 2018.
- Hansen, N., Lin, Y., Su, H., Wang, X., Kumar, V., and Rajeswaran, A. Modem: Accelerating visual model-based reinforcement learning with demonstrations. *arXiv preprint arXiv:2212.05698*, 2022.
- Haykin, S. *Neural networks: a comprehensive foundation*. Prentice Hall PTR, 1998.
- Hendrycks, D. and Gimpel, K. Gaussian error linear units (gelus). *arXiv preprint arXiv:1606.08415*, 2016.
- Hester, T., Vecerik, M., Pietquin, O., Lanctot, M., Schaul, T., Piot, B., Horgan, D., Quan, J., Sendonaris, A., Osband, I., et al. Deep q-learning from demonstrations. In *Proceedings of the AAAI conference on artificial intelligence*, volume 32, 2018.
- Hu, H., Yang, Y., Ye, J., Wu, C., Mai, Z., Hu, Y., Lv, T., Fan, C., Zhao, Q., and Zhang, C. Bayesian design principles for offline-to-online reinforcement learning. *arXiv preprint arXiv:2405.20984*, 2024.
- James, S., Ma, Z., Arrojo, D. R., and Davison, A. J. Ribench: The robot learning benchmark & learning environment. *IEEE Robotics and Automation Letters*, 5(2):3019–3026, 2020.
- Kumar, A., Zhou, A., Tucker, G., and Levine, S. Conservative q-learning for offline reinforcement learning. *Advances in Neural Information Processing Systems*, 33: 1179–1191, 2020.
- Lee, S., Seo, Y., Lee, K., Abbeel, P., and Shin, J. Offline-to-online reinforcement learning via balanced replay and pessimistic q-ensemble. In *Conference on Robot Learning*, pp. 1702–1712. PMLR, 2022.
- Lei, K., He, Z., Lu, C., Hu, K., Gao, Y., and Xu, H. Uni-o4: Unifying online and offline deep reinforcement learning with multi-step on-policy optimization. *arXiv preprint arXiv:2311.03351*, 2023.
- Li, Z., Liu, F., Yang, W., Peng, S., and Zhou, J. A survey of convolutional neural networks: analysis, applications, and prospects. *IEEE transactions on neural networks and learning systems*, 33(12):6999–7019, 2021.
- Lillicrap, T. Continuous control with deep reinforcement learning. *arXiv preprint arXiv:1509.02971*, 2015.
- Metz, L., Ibarz, J., Jaitly, N., and Davidson, J. Discrete sequential prediction of continuous actions for deep rl. *arXiv preprint arXiv:1705.05035*, 2017.
- Mnih, V., Kavukcuoglu, K., Silver, D., Rusu, A. A., Veness, J., Bellemare, M. G., Graves, A., Riedmiller, M., Fidjeland, A. K., Ostrovski, G., et al. Human-level control through deep reinforcement learning. *nature*, 518(7540): 529–533, 2015.

- Nair, A., McGrew, B., Andrychowicz, M., Zaremba, W., and Abbeel, P. Overcoming exploration in reinforcement learning with demonstrations. In *2018 IEEE international conference on robotics and automation (ICRA)*, pp. 6292–6299. IEEE, 2018.
- Nakamoto, M., Zhai, S., Singh, A., Sobol Mark, M., Ma, Y., Finn, C., Kumar, A., and Levine, S. Cal-ql: Calibrated offline rl pre-training for efficient online fine-tuning. *Advances in Neural Information Processing Systems*, 36, 2024.
- Rajeswaran, A., Kumar, V., Gupta, A., Vezzani, G., Schulman, J., Todorov, E., and Levine, S. Learning complex dexterous manipulation with deep reinforcement learning and demonstrations. *arXiv preprint arXiv:1709.10087*, 2017.
- Rudner, T. G., Lu, C., Osborne, M. A., Gal, Y., and Teh, Y. On pathologies in kl-regularized reinforcement learning from expert demonstrations. *Advances in Neural Information Processing Systems*, 34:28376–28389, 2021.
- Schrittwieser, J., Antonoglou, I., Hubert, T., Simonyan, K., Sifre, L., Schmitt, S., Guez, A., Lockhart, E., Hassabis, D., Graepel, T., et al. Mastering atari, go, chess and shogi by planning with a learned model. *Nature*, 588(7839): 604–609, 2020.
- Schulman, J., Wolski, F., Dhariwal, P., Radford, A., and Klimov, O. Proximal policy optimization algorithms. *arXiv preprint arXiv:1707.06347*, 2017.
- Seo, Y. and Abbeel, P. Reinforcement learning with action sequence for data-efficient robot learning. *arXiv preprint arXiv:2411.12155*, 2024.
- Seo, Y., Uruç, J., and James, S. Continuous control with coarse-to-fine reinforcement learning. *arXiv preprint arXiv:2407.07787*, 2024.
- Seyde, T., Werner, P., Schwarting, W., Gilitschenski, I., Riedmiller, M., Rus, D., and Wulfmeier, M. Solving continuous control via q-learning. *arXiv preprint arXiv:2210.12566*, 2022.
- Seyde, T., Werner, P., Schwarting, W., Wulfmeier, M., and Rus, D. Growing q-networks: Solving continuous control tasks with adaptive control resolution. *arXiv preprint arXiv:2404.04253*, 2024.
- Silver, D., Schrittwieser, J., Simonyan, K., Antonoglou, I., Huang, A., Guez, A., Hubert, T., Baker, L., Lai, M., Bolton, A., et al. Mastering the game of go without human knowledge. *nature*, 550(7676):354–359, 2017.
- Tang, Y. and Agrawal, S. Discretizing continuous action space for on-policy optimization. In *Proceedings of the aaai conference on artificial intelligence*, volume 34, pp. 5981–5988, 2020.
- Tavakoli, A., Pardo, F., and Kormushev, P. Action branching architectures for deep reinforcement learning. In *Proceedings of the aaai conference on artificial intelligence*, volume 32, 2018.
- Tavakoli, A., Fatemi, M., and Kormushev, P. Learning to represent action values as a hypergraph on the action vertices. *arXiv preprint arXiv:2010.14680*, 2020.
- Van Hasselt, H., Guez, A., and Silver, D. Deep reinforcement learning with double q-learning. In *Proceedings of the AAAI conference on artificial intelligence*, volume 30, 2016.
- Yan, Z., Zhang, H., Piramuthu, R., Jagadeesh, V., DeCoste, D., Di, W., and Yu, Y. Hd-cnn: hierarchical deep convolutional neural networks for large scale visual recognition. In *Proceedings of the IEEE international conference on computer vision*, pp. 2740–2748, 2015.
- Yarats, D., Fergus, R., Lazaric, A., and Pinto, L. Mastering visual continuous control: Improved data-augmented reinforcement learning. *arXiv preprint arXiv:2107.09645*, 2021.
- Yu, C., Velu, A., Vinitisky, E., Gao, J., Wang, Y., Bayen, A., and Wu, Y. The surprising effectiveness of ppo in cooperative multi-agent games. *Advances in Neural Information Processing Systems*, 35:24611–24624, 2022.
- Zhang, H., Xu, W., and Yu, H. Policy expansion for bridging offline-to-online reinforcement learning. *arXiv preprint arXiv:2302.00935*, 2023.
- Zhao, T. Z., Kumar, V., Levine, S., and Finn, C. Learning fine-grained bimanual manipulation with low-cost hardware. *arXiv preprint arXiv:2304.13705*, 2023.
- Ziebart, B. D., Maas, A. L., Bagnell, J. A., Dey, A. K., et al. Maximum entropy inverse reinforcement learning. In *Aaai*, volume 8, pp. 1433–1438. Chicago, IL, USA, 2008.

A. Proof of Theorem 4.3

First, we express the policy using conditional probability, and then replace it with Eq. (11).

$$\begin{aligned}
 \pi(\mathbf{a}|\mathbf{s}) &= \prod_{d=1}^D \pi(a^d|\mathbf{s}, \mathbf{a}^{-d}) \\
 &= \prod_{d=1}^D \frac{\exp\left(\frac{1}{\alpha} A^d(\mathbf{s}, \mathbf{a}^{-d}, a^d)\right)}{Z(\mathbf{s}, \mathbf{a}^{-d})} \\
 &= \frac{\prod_{d=1}^D \exp\left(\frac{1}{\alpha} A^d(\mathbf{s}, \mathbf{a}^{-d}, a^d)\right)}{\prod_{d=1}^D Z^d(\mathbf{s}, \mathbf{a}^{-d})} \\
 &= \frac{\exp\left(\frac{1}{\alpha} \sum_{d=1}^D A^d(\mathbf{s}, \mathbf{a}^{-d}, a^d)\right)}{\prod_{d=1}^D Z^d(\mathbf{s}, \mathbf{a}^{-d})}
 \end{aligned} \tag{19}$$

We can then apply Eq. (12), resulting in

$$\pi(\mathbf{a}|\mathbf{s}) = \exp\left(\frac{1}{\alpha} \sum_{d=1}^D A^d(\mathbf{s}, \mathbf{a}^{-d}, a^d)\right) \tag{20}$$

Recall that the policy $\pi(\mathbf{a}|\mathbf{s})$ can be represented using the soft advantage as shown in Eq. (10). Therefore, we have

$$\sum_{d=1}^D A^d(\mathbf{s}, \mathbf{a}^{-d}, a^d) = A(\mathbf{s}, \mathbf{a}) \tag{21}$$

B. Implementation Details

B.1. Action Selection

As illustrated in Algorithm 1, the action selection process receives inputs from A_{θ_1} and A_{θ_2} and produces \mathbf{a}_t . Eq. (10) and Eq. (16) describe the action selection process utilizing a single soft advantage network. To leverage the benefits of a double network, we employ two advantage networks to generate more precise actions. This process is detailed in Algorithm 2.

Algorithm 2 ARSQ Action Selection with Double Q Network

Input: parameter $\theta_{1,2}$ for A^{θ_i} , state \mathbf{s}_t
Output: action \mathbf{a}_t
 Initialize output action $\mathbf{a}_t = \emptyset$
for each action dimension d **do**
 Compute $A^{d,\theta_i}(\mathbf{s}_t, \mathbf{a}_t, a^d)$ for each a^d (16)
 Compute $A^d(a^d) = \min_i A^{d,\theta_i}(\mathbf{s}_t, \mathbf{a}_t, a^d)$
 Compute $\tilde{\pi}^d(a^d) = \exp\left(\frac{1}{\alpha} A^d(a^d)\right)$ (10)
 Normalize $\tilde{\pi}^d$ by $\pi^d(a^d) = \frac{\tilde{\pi}^d(a^d)}{\sum_{a^{d'}} \tilde{\pi}^d(a^{d'})}$
 Sample discrete action at dimension d with $\pi^d(a^d)$
 Append action $\mathbf{a}_t = \mathbf{a}_t \cup \{a^d\}$
end for

B.2. Variant of Behavior Cloning Objective

As discussed in Sec. 4.3, we incorporate an behavior cloning objective to effectively utilize offline demonstration data during online training, as defined in Eq. (15).

Following prior works (Kumar et al., 2020), we also employ a variant of this objective, expressed as:

$$\mathcal{L}_{BC-v}^d = \max \left(\log \sum_{a^d \neq a_e^d} \exp(A^{d,\theta_i}(\mathbf{s}, \mathbf{a}_e^{-d}, a^d)) - A^{d,\theta_i}(\mathbf{s}, \mathbf{a}_e^{-d}, a_e^d), C_m \right) \tag{22}$$

where a_e^d is the expert action and C_m is a predefined margin constant.

We observe that this variant objective achieves better performance in scenarios where action modes are concentrated, such as in the *medium* and *medium-expert* series of datasets in D4RL. Consequently, we adopt this variant objective when working with such datasets.

B.3. Network Architecture

In RL Bench tasks, observations consist of a combination of RGB images and low-dimensional states. To compute the dimensional soft advantage for a given dimension, we first input the RGB images and low-dimensional states into a Convolutional Neural Network (CNN) (Li et al., 2021) encoder and a Multi-Layer Perceptron (MLP) (Haykin, 1998) encoder, respectively, to extract feature representations. These representations are then used to predict the soft value. Concurrently, the feature representations are combined with actions from previous dimensions and coarse-to-fine levels to create auto-regressive conditioning. An MLP-based shared backbone and output head are then utilized to determine the dimensional soft advantage for the given dimension.

In D4RL tasks, observations consist solely of low-dimensional states, and feature representations are derived directly from these states.

B.4. Hyper-parameters

Hyper-parameter	D4RL	RLBench
Image resolution	/	$84 \times 84 \times 3$
Image augmentation	/	RandomShift
Frame stack	1	8
CNN - Encoder	/	Conv (c=[32, 64, 128, 256], s=2, p=1)
Backbone	Linear (512, 512, 512)	Linear (512, 512, 512, bias=False)
Output Head Layers	1	1
Activation	Tanh	SiLU & LayerNorm
Coarse-to-fine Levels	2	3
Coarse-to-fine Bins	7	5
Batch Size	512	512
Optimizer	Adam	AdamW (weight decay = 0.1)
Learning Rate	3e-4	5e-5
Temperature Coefficient α	0.01	0.001
Target Critic Update Ratio (τ)	0.005	0.02
BC Margin C_m	-1	-0.01
Action Roll-out Network	Current	Target

Table 1. Typical hyper-parameters of ARSQ in D4RL and RL Bench.

The hyperparameters of ARSQ are presented in Table 1. We provide the typical hyperparameters for ARSQ in D4RL (*hopper-medium*) and RL Bench (*Open Oven*). In RL Bench, ARSQ employs RandomShift (Yarats et al., 2021) for image augmentation. Additionally, ARSQ utilizes SiLU (Hendrycks & Gimpel, 2016) and LayerNorm (Ba, 2016) as activation functions in RL Bench.

C. Experiment Setup

C.1. Motivating Example Setup

As introduced in Sec. 1 and illustrated in Fig. 1, we consider a motivating example to demonstrate the impact of Q decomposition on policy training. The dataset is depicted in Fig. 1a, with each point to be a data point in the dataset. The color of the data points indicates the reward of the data point. To illustrate the Q function of value-based RL algorithms, we first discretize the action space with 2 bins in each action dimension.

- Q function given by independent action decomposition is an example of DecQN (Seyde et al., 2022), as well as in CQN (Seo et al., 2024), which features just a single coarse-to-fine level. In this setting, we employ separate tabular Q functions, $Q(s, a_1)$ and $Q(s, a_2)$, for action dimension 1 and action dimension 2. The Q function is learned by gradient descent.
- For the Q function obtained through auto-regressive action decomposition, we employ both tabular soft advantage functions, $A^1(s, a_1)$ and $A^2(s, a_1, a_2)$ for action dimension 1 and action dimension 2, and a tabular soft value function $V_{\text{soft}}(s)$. The Q value reported in Fig. 1c is a sum of the soft value and the dimensional soft advantage of the corresponding dimensions, i.e., $Q(s, a_1, a_2) = V_{\text{soft}}(s) + A^1(s, a_1) + A^2(s, a_1, a_2)$. The soft advantage functions and the soft value function are simultaneously learned through gradient descent.

C.2. Environment and Dataset

D4RL Gym Environment D4RL (Fu et al., 2020) provides datasets for various tasks to evaluate the performance of reinforcement learning. In this context, we use 3 Gym Locomotion tasks and datasets from D4RL to assess the performance of ARSQ and other baselines. These tasks are illustrated in Fig. 9. The agent’s observations include its states, such as the angle and velocity of each rotor. The agent’s actions consist of torques applied between the robot’s links, constrained within the range of $(-1, 1)$. The reward is dense, offering incentives for task completion and survival, while penalizing excessive energy-consuming actions.

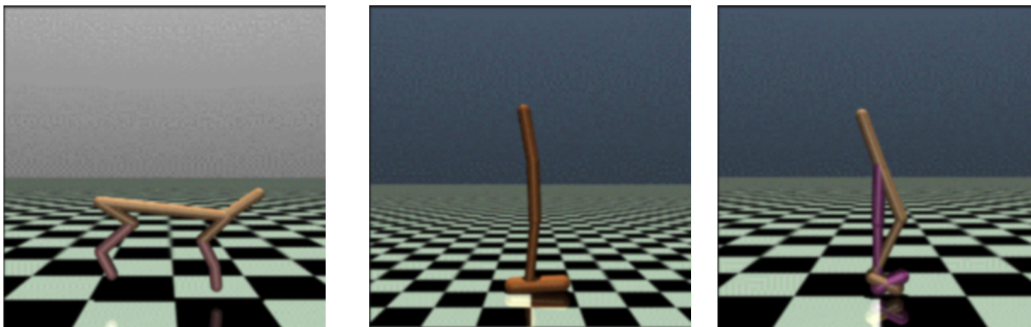


Figure 9. D4RL Gym tasks used in experiment.

D4RL Dataset In D4RL, we use the *medium-replay*, *medium*, and *medium-expert* datasets for tasks involving *half-cheetah*, *hopper*, and *walker2d*. In Section 5.1, to examine the impact of dataset quality, we rank trajectories based on episode returns within these nine datasets. Specifically, we compute the total reward for each data chunk within each dataset. We then rank these data chunks and select the top, middle, and bottom 30% accordingly. This is akin to rank trajectories but is easier to handle.

To better demonstrate the suboptimal nature of the datasets, we have plotted a histogram of the data chunk rewards, as shown in Fig. 10.

RLBench Environment RLBench (James et al., 2020) serves as a benchmark and learning environment for robot control. We have selected 20 tasks from RLBench and present results for 6 of them in Sec. 5. An illustration of the environment can be seen in Fig. 11. The input consists of RGB images with a resolution of 84×84 , captured from four camera angles: front, wrist, left-shoulder, and right-shoulder, along with a history of the past seven observations. The output specifies the change in joint angles at each time step, utilizing the delta JointPosition mode provided by RLBench. In our experiments, we use a binary sparse reward system (0 or 1), which is awarded only at the final timestamp of an episode to indicate task success.

C.3. Baselines and Evaluation Details

Main results baselines. As mentioned in Sec. 5.1, within D4RL, we utilize the implementation from (Seo et al., 2024) and modify its CNN-based encoder to an MLP-based encoder as the CQN baseline. The BC baseline originates from CQN but operates with the RL learning objective turned off and without any online environment interaction.

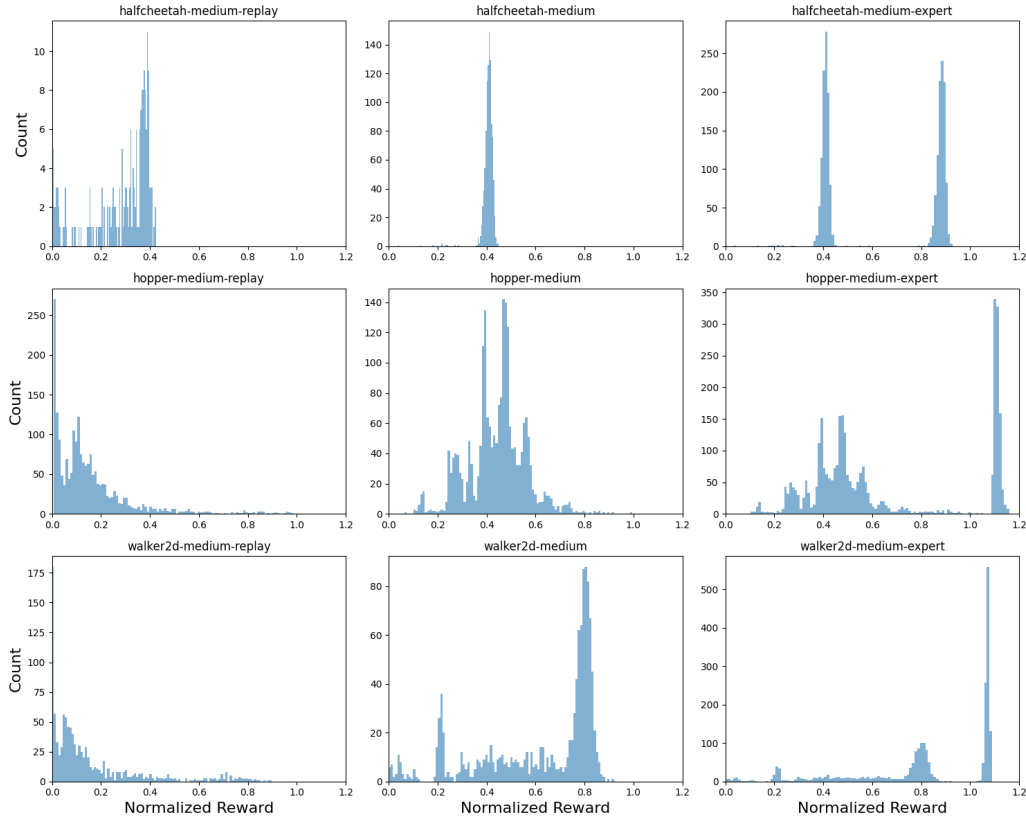


Figure 10. Histogram of reward in D4RL datasets.

In RLbench, we use the baselines and results of CQN, DrQ-v2+, DrQ-v2, ACT, and CBC as reported in the original CQN paper (Seo et al., 2024).

Ablation study baselines. As mentioned in Sec. 5.3, we utilize the *Separate* and *Level Shared* backbone baselines for an ablation study to explore the effectiveness of the shared backbone in the advantage network. The network architectures of these two baselines are illustrated in Fig. 12 and Fig. 13.

D. Additional Results

Sensitivity of temperature coefficient α . Our methods are derived from Soft Q-learning, which aims to achieve a maximum-entropy policy. The temperature coefficient α in Eq. (1) affects the balance between maximizing policy entropy and the reward from the environment. We conducted experiments to examine how varying α impacts policy learning.

As shown in Fig. 14, a very high α results in reduced performance and unstable training, whereas a very low α also hampers policy improvement by restricting exploration.

D4RL results per task for different demonstration quality. In Sec. 5.1, we present the D4RL results, averaged over all 9 datasets, based on varying demonstration quality. The results for each task are illustrated in Fig. 15. ARSQ consistently outperforms the CQN and BC baselines in nearly every task, demonstrating its ability to maintain stable performance across datasets of varying quality.

RLBench results in all 20 tasks. In Sec. 5.2, we present results for six selected tasks from RLbench. The complete results for all 20 tasks are displayed in Fig. 16. These results indicate that ARSQ performs comparably or better across these tasks, showcasing its ability to learn effectively even when the data collected online is not optimal.

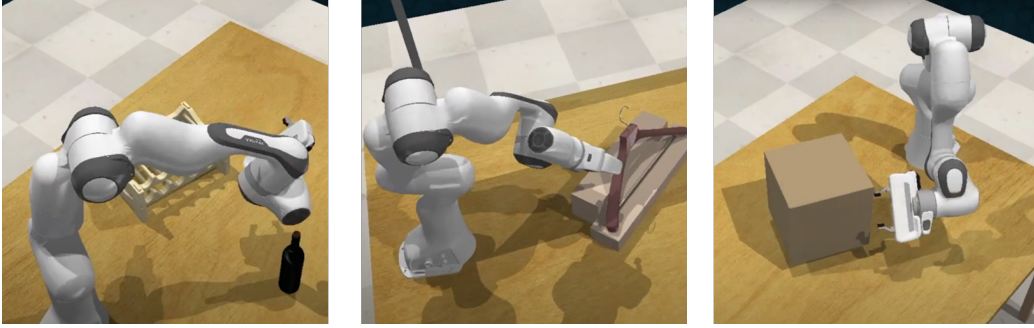
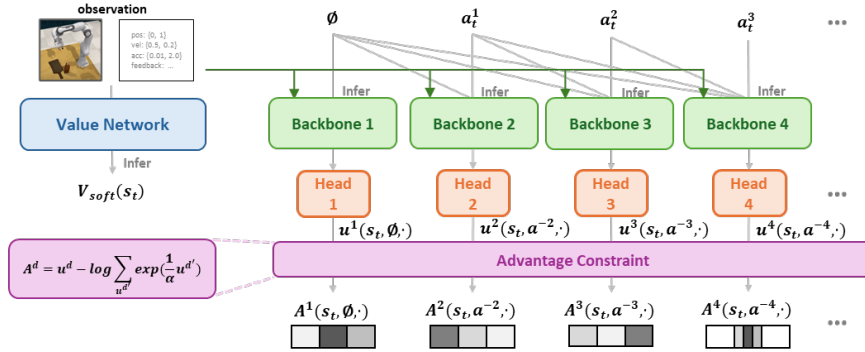


Figure 11. Example of RL Bench tasks used in experiment.


 Figure 12. Network architecture of *Separate* backbone baseline in ablation study.

E. Computational Cost Analysis

As discussed in Sec. 4.3, ARSQ generates actions in each dimension in an auto-regressive manner. To analyze the overhead, we conducted experiments on both D4RL (*hopper-medium*) and RL Bench (*Open Oven*) tasks. The training and inference times for ARSQ and CQN were evaluated 1,000 times and averaged. These experiments were conducted on a single Nvidia RTX 3090 graphics card.

The results are shown in Fig. 2. ARSQ exhibits similar training times to CQN, due to the parallel optimization implemented and the batch training nature of the auto-regressive model. However, ARSQ experiences higher inference latency compared to CQN. We aim to address this issue by grouping the action dimensions and outputting the grouped dimensional actions auto-regressively, a solution we plan to explore in future work.

	D4RL	RLBench
ARSQ Inference	4.1	32.1
ARSQ Training	12.2	290.5
CQN Inference	2.6	6.9
CQN Training	11.6	260.5

Table 2. Computational time in D4RL and RL Bench (ms).

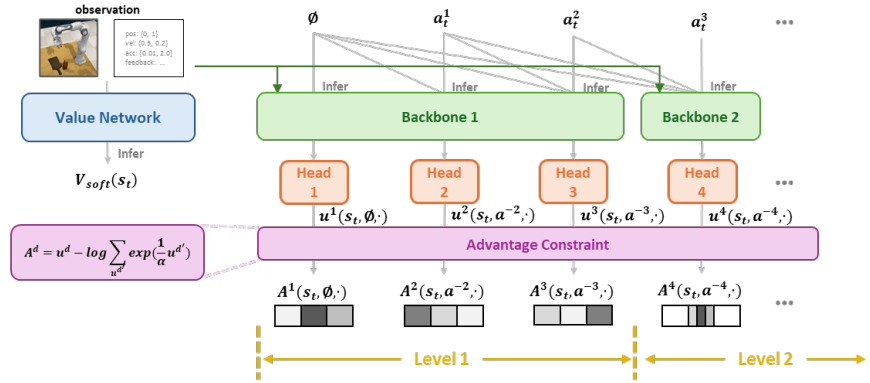


Figure 13. Network architecture of Level Shared backbone baseline in ablation study.

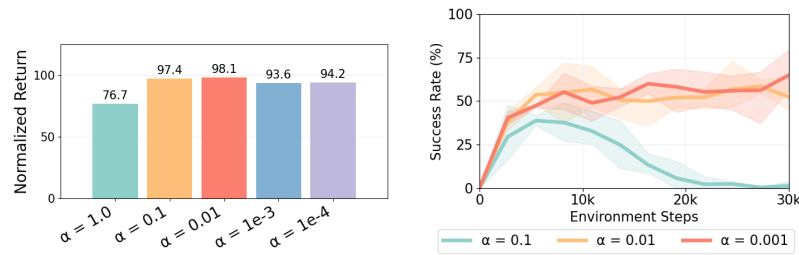


Figure 14. Sensitivity of temperature coefficient α in D4RL and RL Bench.

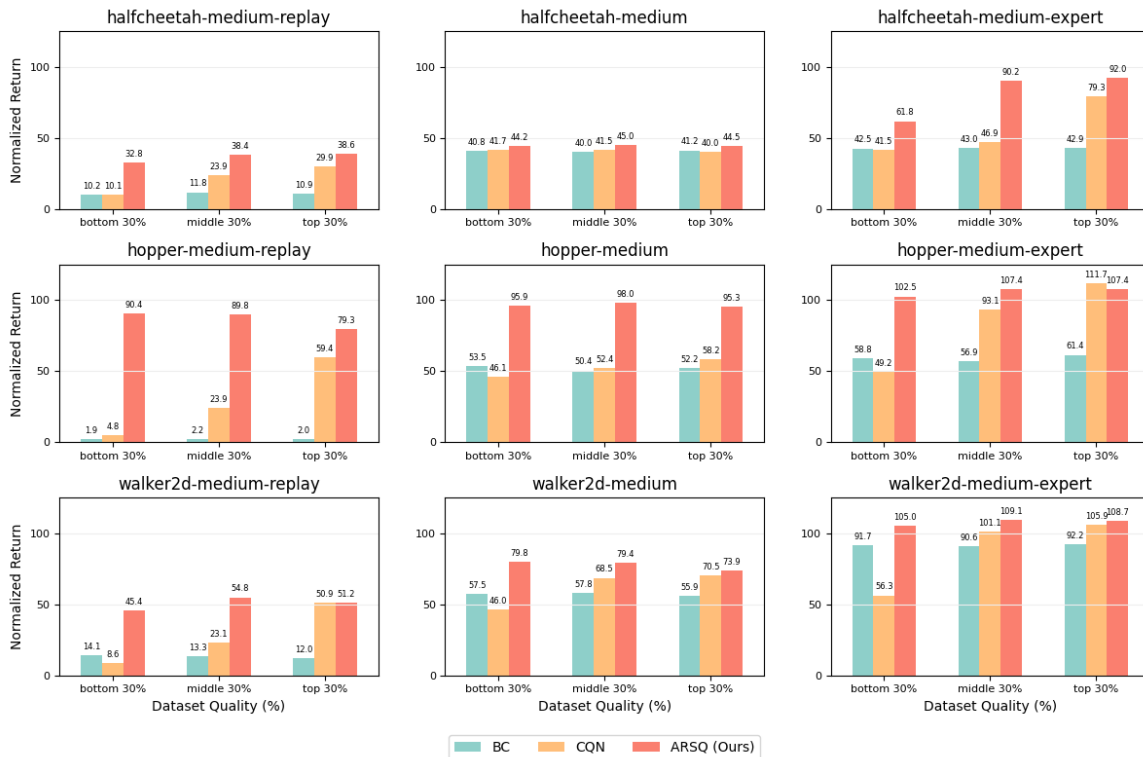


Figure 15. D4RL results per task on different demonstration quality.

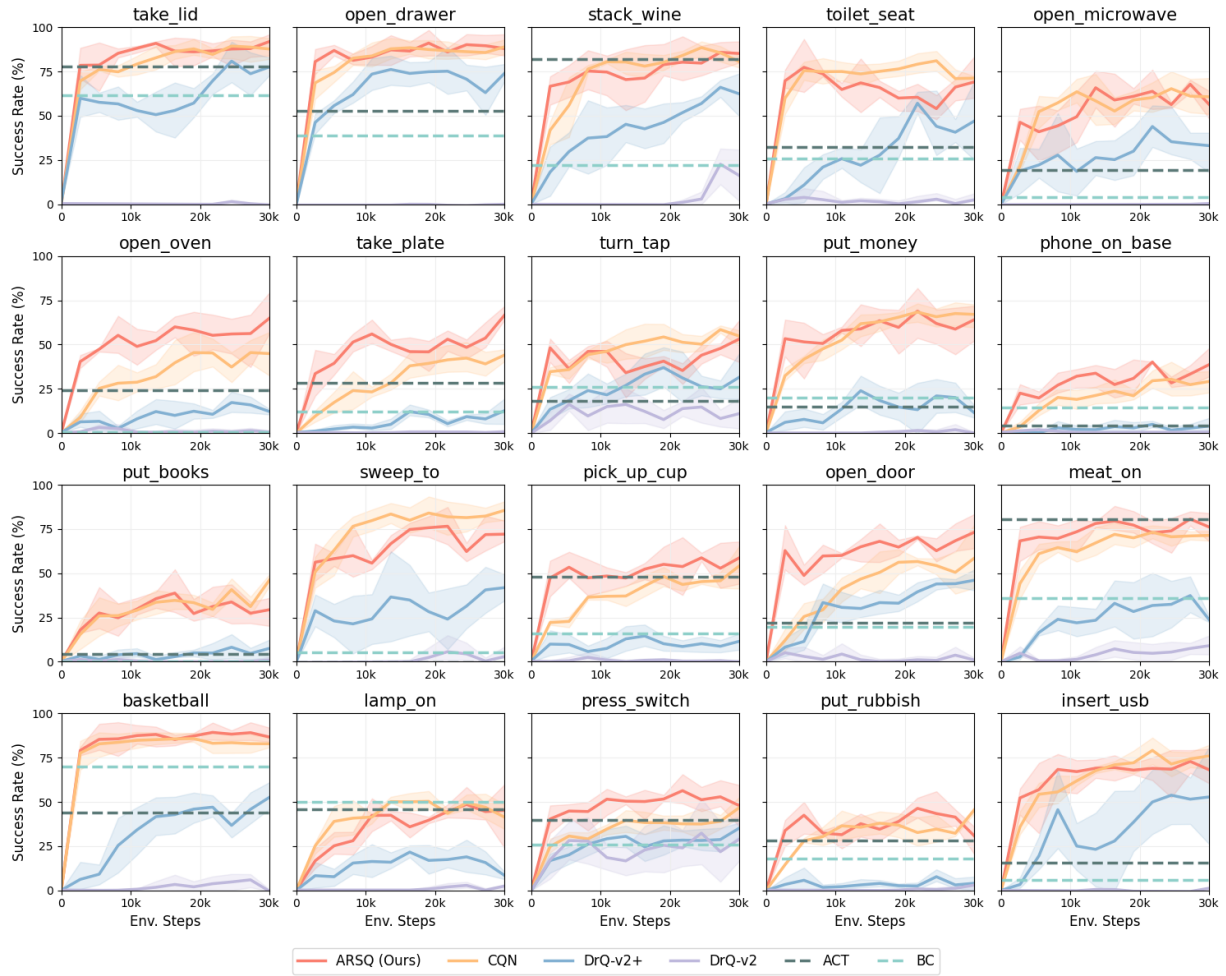


Figure 16. RLBench results in all 20 tasks.